Earth and Planetary Science Letters 493 (2018) 208–217

Contents lists available at ScienceDirect

Earth and Planetary Science Letters

www.elsevier.com/locate/epsl

Application of combined ^{81}Kr and ^{4}He chronometers to the dating of old groundwater in a tectonically active region of the North China Plain

Takuya Matsumoto [a,*], Zongyu Chen [b], Wen Wei [b], Guo-Min Yang [c], Shui-Ming Hu [c], Xiangyang Zhang [b]

[a] Isotope Hydrology Section, Division of Physical and Chemical Sciences, Department of Nuclear Sciences and Applications, International Atomic Energy Agency, Vienna International Centre, PO Box 100, 1400 Vienna, Austria
[b] Institute of Hydrogeology and Environmental Geology (IHEG), Chinese Academy of Geological Sciences, 050061, Shijiazhuang, China
[c] Hefei National Laboratory for Physical Sciences at Microscale, iChem Center, University of Science and Technology of China, Hefei, Anhui 230026, China

ARTICLE INFO

Article history:
Received 13 December 2017
Received in revised form 19 April 2018
Accepted 20 April 2018
Available online xxxx
Editor: D. Vance

Keywords:
groundwater dating
noble gas
^{4}He
^{81}Kr
atom trap trace analysis
North China Plain

ABSTRACT

Groundwater dating by radio-krypton (^{81}Kr; half-life of about 229,000 years) was applied to the sedimentary basin aquifer of the North China Plain (NCP). Krypton gas extracted from deep groundwater in the Coastal Plain was analyzed for ^{81}Kr/Kr ratios by Atom Trap Trace Analysis, which yielded normalized ratios of 0.05 to 0.20, corresponding to groundwater residence times of 0.5–1 million years. Helium isotope compositions were determined on groundwater samples collected from the Central Plain and the Coastal Plain along a flow path of about 200 km. Helium dissolved in the groundwater samples are a mixture of atmospheric, crustal radiogenic and mantle derived sources. Mantle derived ^{3}He contributes up to 30% of the total, and the area of occurrence coincides with zones of previous magmatic/tectonic activities. By contrast, >90% of ^{4}He is derived from crustal reservoirs and correlates with ^{81}Kr ages. The absolute groundwater ages (^{81}Kr) and radiogenic ^{4}He concentrations permit us to calibrate the ^{4}He flux into the aquifer as well as the vertical diffusion rate of ^{4}He to utilize the radiogenic ^{4}He in groundwater as a quantitative age tracer. Previously, groundwater showed ^{14}C activities near the limit of detection (30–40 k yr), in contrast Kr and radiogenic ^{4}He data reveal progressively older ages from the recharge area to the Coastal Plain, from <20,000 yr to 0.5 to 1 Ma along the flow path of the NCP aquifers.

1. Introduction

Accumulation of radiogenic helium (^{4}He) derived from the decay of U and Th in deep groundwater has been used to obtain groundwater residence time (e.g., Andrews, 1985; Aeschbach-Hertig et al., 2002; Plummer et al., 2012; Kulongoski et al., 2008; Aggarwal et al., 2015; Wen et al., 2016). ^{4}He has potential to date water over timescales of thousands to millions of years. However, external ^{4}He sources to aquifers (basal fluxes entering the bottom of aquifers) and difficulties with the quantification of He release rates from host rock to water have hampered its use. Thus the ^{4}He method requires 'calibration' using other radionuclides. Until recently, ^{4}He ages were calibrated using ^{14}C ages (e.g., Plummer et al., 2012), but the shorter half-life of ^{14}C often leads to inaccurate age estimates in groundwater older than ~30,000 yr (Aggarwal et al., 2015).

In this context, recent advances in Atom trap trace analysis (e.g., Lu et al., 2014) has enabled the application of krypton-81 (^{81}Kr; half-life 229,000 yr) as a tool to date very old groundwater (e.g., Lehmann et al., 2003; Sturchio et al., 2004; Aeschbach-Hertig, 2014). As a noble gas, Kr is non-reactive and is derived solely from atmospheric sources. Its long half-life and the lack of geochemical interactions make this radionuclide an ideal tracer to estimate groundwater ages in deep aquifer systems.

^{81}Kr offers the possibility of 'calibrating' the ^{4}He chronometer to facilitate application to groundwater beyond the ^{14}C age range. The first application of combined ^{81}Kr and ^{4}He age proxies was done on the Guarani aquifer in Brazil (Aggarwal et al., 2015), in which ^{81}Kr was used to constrain model parameters to convert ^{4}He concentrations in groundwater into ages. Here, we expand the use of these isotopic tracers to a deep aquifer in a tectonically active area of the North China Plain (NCP) – the largest alluvial plain in eastern Asia. We targeted areas where previous studies identified significant contributions of mantle-derived helium in relatively old groundwaters (Wei et al., 2015). In the NCP,

* Corresponding author.
E-mail address: t.matsumoto@iaea.org (T. Matsumoto).

https://doi.org/10.1016/j.epsl.2018.04.042
0012-821X/

Table 1
The main aquifers of the NCP.

Strata	Depth to the bottom of aquifers (m)		Groundwater	Lithology
Quaternary	~50	I	Saline, TDS > 5 g/L	Silt, clay, and fine sand interbed
	50–150	II	Saline, TDS > 5 g/L	
	150–350	III	Fresh, TDS < 1 g/L	
	350–450	IV	Fresh, TDS < 1 g/L	
Neogene (Minghuazhen group)	600–680	V1	Brackish, TDS 1–1.5 g/L	Clay, medium sand, fine sand
	740–820	V2	Brackish, TDS ~1.5 g/L	Mudstone, sandstone, and conglomerate sandstone
	900–1100	V3	Brackish (Geothermal), TDS ~1.5 g/L	

there have been attempts to estimate residence times of the deep confined aquifer using ^{14}C (Wei et al., 2015) and ^{36}Cl (Dong et al., 2002). These efforts identified residence times beyond the limits of the ^{14}C method (~35 kyr) to hundreds of thousands of years (^{36}Cl). Concentrations of ^{4}He varied by more than a factor of 10 among groundwater samples with <2 pMC (percent of modern carbon) of ^{14}C (Kreuzer et al., 2009; Wei et al., 2015), implying that ^{4}He concentrations represented accumulation beyond the application limit of the ^{14}C method. In fact, conceptual modeling suggested that the deep confined aquifer could have residence times approaching 1 Myr (Cao et al., 2016). At such time scales ^{14}C and ^{36}Cl are unreliable tracers, and the ^{81}Kr age method could provide better insight into the renewability of groundwaters in the NCP, given high contemporary rates of groundwater exploitation.

2. Study area

The NCP overlies a thick Cenozoic sedimentary basin covering ~150,000 km^2, and consists of the piedmont pluvial plain, the central alluvial and flood plain, and the coastal plain (Fig. 1a). It is one of the most densely populated areas of the world and is of great agricultural importance for China. The regional aquifer system consists of thick Neogene and Quaternary deposits. These sediments are dominated by alluvial and lacustrine deposits with interbedded marine deposits in the littoral plain. The aquifer system of the Quaternary–Pliocene formations consists of five aquifers (Table 1 and Fig. 1b). Aquifer I, is a phreatic aquifer around 10–20 m thick, consisting of fine-grained sand in the littoral plain. Depth to the groundwater table is ~2–3 m, and the specific yield is about 1–2.5 m^3/h m. Groundwater is a Na–Cl type with TDS >5 g/L (maximum value of 9 g/L). Aquifer II, depth to ~150 m consists of fine sand and silt. Groundwater is Na–Cl type with TDS 7–8 g/L. Aquifer III and aquifer IV are hydraulically connected and are the target of present resource exploitation. Aquifer III, depth to ~350 m and about 25–60 m thick, is a confined aquifer consisting of fine sand. The specific yield is about 5–10 m^3/h m. Groundwater is Na–Cl–HCO_3 type with TDS <1 g/L. Fluoride concentrations range up to 5.5–6.9 mg/L. Aquifer IV, depth to ~550 m, with a thickness of 20–50 m, consists of fine sand and silt. The specific yield is less than 2.5 m^3/h m. Groundwater is Na–Cl–HCO_3 type with TDS <1 g/L. The fluoride concentration is up to 2.5–3.5 mg/L. Aquifer V (subdivided into V1 to V3), depth to ~1100 m, is a Pliocene confined aquifer consisting of fine sand and silts in the upper part of this group, and mudstone, sandstone and conglomerate sandstone in the lower part of this group. This aquifer is mainly exploited around Huanghua city. The deposits of subgroup aquifer V1, depth at above 680 m, consist of 8–12 layers of alluvial and lacustrine fine sands with a total thickness of ~70 m. Groundwater is HCO_3–Na type with TDS 1.15–1.48 g/L. The fluoride concentration is about 2 mg/L. The deposit of subgroup aquifer V2, depth at above 820 m, consists of sandstone with a total thickness of ~50 m. Groundwater is Na–HCO_3 type with TDS ~1.5 mg/L. The deposit of subgroup aquifer V3, depth at above 1100 m, consists of well cemented sandstone with a total thickness of ~100 m. Groundwater is Na–Cl–HCO_3 type with TDS 0.8–1.5 mg/L. Some geothermal water, with temperatures of 30–50 °C, occurs in this reservoir. Further details of the NCP aquifer system can be found elsewhere (Zhang et al., 2000; Chen et al., 2003; Kreuzer et al., 2009).

3. Sampling and measurements

This study focused on confined aquifer (III to V) along the general east to west flow line in a middle of the Central Plain to the Coastal Plain. Groundwater samples for stable noble gases (He and Ne) were collected in copper tubes with stainless steel pinch clamps (Weiss, 1968) from 20 wells (Fig. 1b) from the Central and Coastal areas of the NCP in 2014 and 2016. Noble gases were analyzed at the Isotope Hydrology Laboratory at the International Atomic Energy Agency using the methods described by Suckow et al. (2008) and Matsumoto et al. (2017). Dissolved gas samples for radio-krypton (^{81}Kr) analysis were collected from five locations in the coastal area using a vacuum cylinder extraction method (Purtschert et al., 2013; Yang et al., 2015). Krypton was purified from co-existent dissolved permanent and biogenic gases by molecular sieve absorption and gas chromatographic methods (Tu et al., 2014). Abundance ratios of purified $^{81}Kr/Kr$ were analyzed by Atom Trap Trace Analysis at University of Science and Technology of China with a method described in Yang et al. (2013).

4. Noble gas results

4.1. Helium concentrations and $^{3}He/^{4}He$ ratios

Table 2 presents results of noble gas analysis by sampling site. The groundwater samples from the NCP have a range of helium concentrations, spanning from 6×10^{-8} cm^3 STP/g to 7×10^{-5} cm^3 STP/g. As shown in Fig. 2a, these concentrations increase towards the coastal plain area, and the new data extend the trends defined by a previous study that covered the area closer to the recharge area (Kreuzer et al., 2009). Isotope ratios of helium ($^{3}He/^{4}He$) from this study and those by Kreuzer et al. (2009) show a monotonic decrease from the recharge area to the middle of the central plain area, and minimum of about 1.1×10^{-7} in well H1201 (Fig. 2b). Thereafter, $^{3}He/^{4}He$ ratios increase towards the coastal plain.

Plotting $^{3}He/^{4}He$ ratios versus Ne/He ratios reveals the involvement of three isotopically and elementally distinctive components in the NCP groundwater samples (Fig. 3a). Except for data with tritiogenic ^{3}He, which is evident from $^{3}He/^{4}He$ ratios greater than the atmospheric ratios, samples from the Piedmont area and the

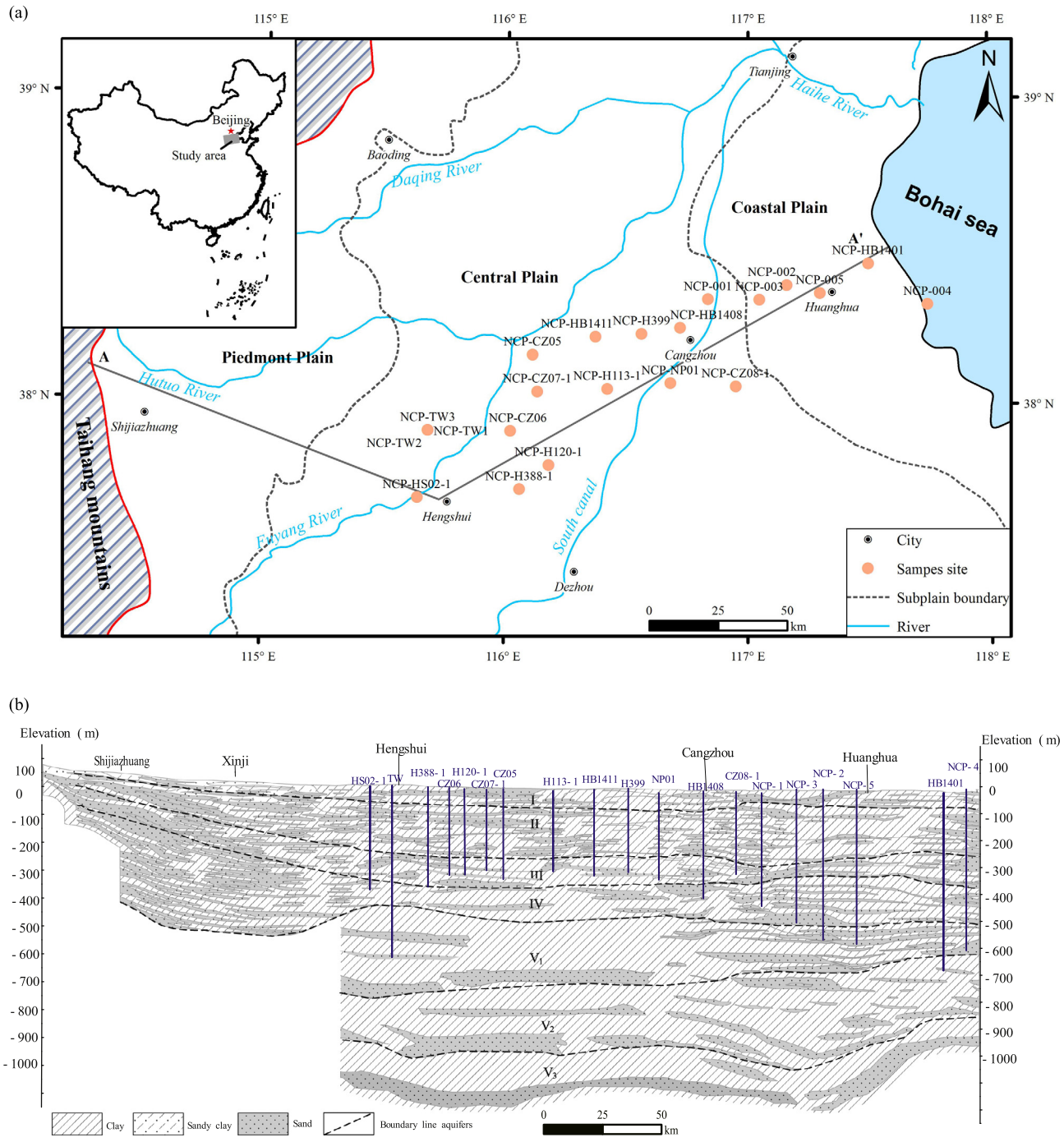

Fig. 1. The study area and sample sites in the North China Plain (a), and a geological cross section of study area and North China Plain (b). The sampled wells are shown as vertical lines.

western part of the Central Plain (i.e., $^3He/^4He > \sim 2 \times 10^{-7}$) nearly all plot along a two component mixing line between atmospheric and crustal radiogenic sources. The remaining samples show a systematic departure from this binary mixing trend to a source component with elevated $^3He/^4He$ and low Ne/He ratios, revealing additional mantle components in those groundwater samples.

4.2. Component separation

Contributions from three different He sources (mantle, crustal radiogenic, and air) can be quantified by solving mixing equations;

$$\left.\begin{aligned} &(^3He/^4He)_{Measured} \\ &\quad = k(^3He/^4He)_{Air} + l(^3He/^4He)_{Mantle} + m(^3He/^4He)_{Crust} \\ &(Ne/^4He)_{Measured} \\ &\quad = k(Ne/^4He)_{Air} + l(Ne/^4He)_{Mantle} + m(Ne/^4He)_{Crust} \\ &1 = k + l + m \end{aligned}\right\} \quad (1)$$

where k, l, and m denote fractions of air, mantle and crustal ^4He components, respectively. With $^3He/^4He$ ratios of air, mantle and crustal components of 1.38×10^{-6}, 1×10^{-5} and 2×10^{-8} and Ne/He ratio of 4 (air equilibrated water at 20 °C), 5×10^{-5} (Graham, 2002) and 5×10^{-8} (Yatsevich and Honda, 1997), respec-

Table 2
Results of noble gas isotope analysis and resultant groundwater ages from ^{81}Kr and ^{4}He.

Sample	Sample date	Longitude	Latitude	Depth (m) (Aquifer)	Altitude (m, asl)	Mass spectrometer results			ATTA results	Groundwater ages (10^5 yr)	
						He (10^{-6} cm^3 STP/g)	Ne (10^{-7} cm^3 STP/g)	^{3}He/^{4}He ($\times 10^{-6}$)	^{81}Kr/Kr (R_{sample}/R_{air})[a]	^{81}Kr ages	^{4}He model age[b]
NCP-001	2013-11-18	116.50	38.20	420(IV)	10	33.8 (±0.8)	2.40 (±0.06)	0.419 (±0.005)	0.200 (+0.032/−0.028)	5.3 (+0.4/−0.4)	6.8
NCP-002	2013-11-20	117.09	38.23	530(V1)	4	37.3 (±0.9)	2.09 (±0.08)	0.340 (±0.004)	0.114 (+0.021/−0.018)	7.2 (+0.5/−0.5)	6
NCP-003	2013-11-20	117.02	38.20	460(IV)	8	27.3 (±0.6)	2.49 (±0.10)	0.443 (±0.007)	0.206 (+0.024/−0.024)	5.2 (+0.4/−0.3)	5.5
NCP-004	2013-11-21	117.44	38.19	580(V1)	4	67.0 (±1.6)	2.23 (±0.06)	0.477 (±0.004)	0.050 (+0.016/−0.013)	9.9 (+0.9/−0.9)	10.4
NCP-005	2013-11-21	117.18	38.22	560(V1)	4	30.2 (±0.7)	2.28 (±0.06)	0.236 (±0.002)	0.098 (+0.019/−0.016)	7.7 (+0.5/−0.5)	5.9
NCP-CZ05	2016-05-24	116.11	38.16	400(III)	10	0.60 (±0.01)	2.07 (±0.02)	0.162 (±0.008)			0.81
NCP-CZ06	2016-05-24	116.02	37.91	280(III)	10	0.47 (±0.01)	2.28 (±0.03)	0.182 (±0.004)			0.6
NCP-CZ07-1	2016-05-24	116.13	38.04	280(III)	10	0.73 (±0.02)	2.29 (±0.03)	0.160 (±0.008)			1
NCP-CZ08-1	2016-05-24	116.95	38.06	300(III)	10	0.33 (±0.00)	2.20 (±0.02)	0.251 (±0.011)			0.38
NCP-H113-1	2016-05-25	116.42	38.05	320(III)	10	2.06 (±0.03)	2.35 (±0.03)	0.159 (±0.013)			2
NCP-H120-1	2016-05-25	116.18	37.80	300(III)	10	1.24 (±0.02)	2.36 (±0.03)	0.108 (±0.006)			1.6
NCP-H388-1	2016-05-25	116.06	37.72	350(III)	10	1.47 (±0.02)	2.41 (±0.03)	0.135 (±0.007)			1.6
NCP-H399	2016-05-26	116.56	38.23	280(III)	10	1.89 (±0.03)	2.35 (±0.03)	0.123 (±0.014)			2.1
NCP-HB1401	2016-05-26	117.50	38.46	700(V2)	10	47.3 (±0.7)	2.60 (±0.03)	0.620 (±0.012)			4.8
NCP-HB1408	2016-05-25	116.72	38.25	400(IV)	10	1.28 (±0.02)	Not determined	0.348 (±0.007)			1.4
NCP-HB1411	2016-05-26	116.37	38.22	300(III)	10	0.99 (±0.01)	2.36 (±0.03)	0.124 (±0.004)			1.3
NCP-HS02-1	2016-05-24	115.64	37.69	350(IV)	10	0.34 (±0.00)	2.17 (±0.02)	0.240 (±0.006)			0.4
NCP-NP01	2016-05-25	116.68	38.07	300(III)	10	8.1 (±0.1)	2.31 (±0.03)	0.221 (±0.008)			3.8
NCP-TW1	2016-05-23	115.68	37.91	600(V1)	10	0.107 (±0.00)	3.19 (±0.04)	1.031 (±0.007)			
NCP-TW3	2016-05-23	115.68	37.91	305(III)	10	0.065 (±0.00)	2.70 (±0.03)	1.194 (±0.012)			

[a] ^{81}Kr is expressed in terms of the air-normalized ratio, $R_{sample}/R_{air} = [^{81}\mathrm{Kr/Kr}]_{sample}/[^{81}\mathrm{Kr/Kr}]_{air}$, where Rair is the modern atmospheric ratio, $[^{81}\mathrm{Kr/Kr}]_{air} = 1.10(\pm 0.05) \times 10^{-12}$, measured by ATTA (Du et al., 2003).

[b] ^{4}He model ages are calculated based on the effective ^{4}He flux and vertical helium diffusion rate determined by using ^{81}Kr and ^{4}He results as input parameters of the model (see text).

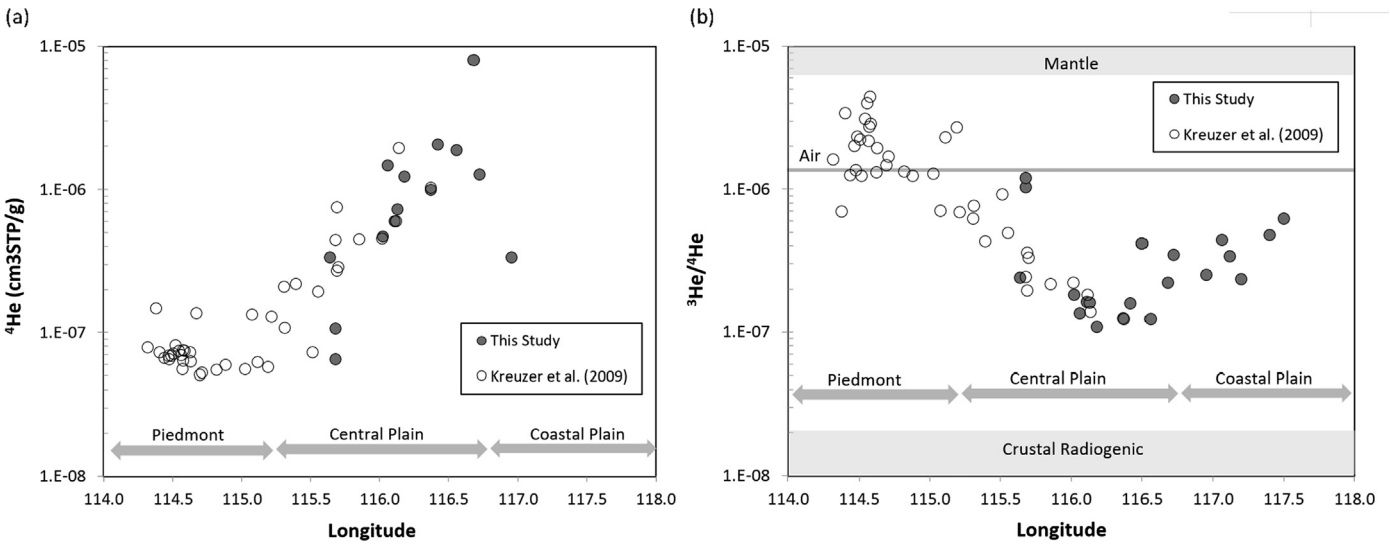

Fig. 2. ^{4}He and ^{3}He/^{4}He ratios of groundwater samples from the North China Plain plotted against longitude of the sampling points. Note that the aquifer flows the eastward, so that flow is from low to high longitude. The groundwater with high ^{3}He/^{4}He ratios in the Piedmont area contains tritiogenic ^{3}He (Kreuzer et al., 2009).

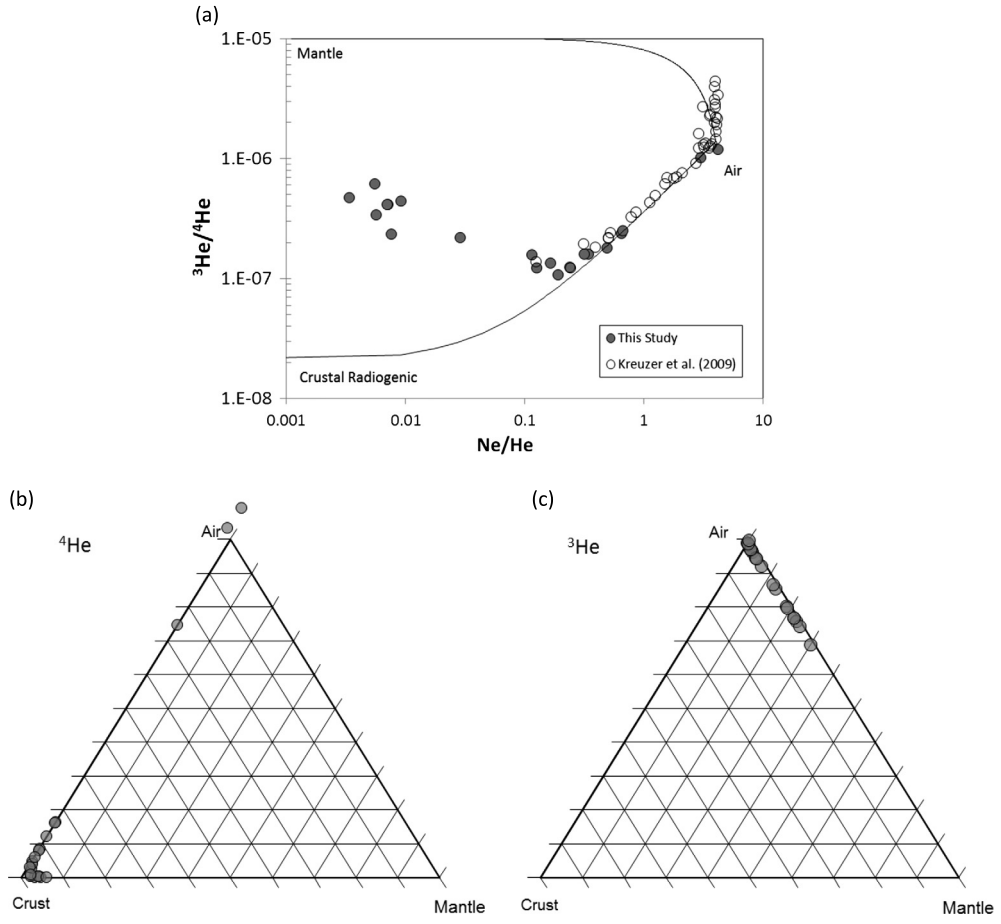

Fig. 3. (a) ^{3}He/^{4}He ratios versus Ne/He ratios, with mixing lines connecting air (Air-equilibrated water), mantle and air and a crustal component. Note that higher ^{3}He/^{4}He ratios near the atmospheric endmember are due to additional tritiogenic ^{3}He, as these are very young groundwaters (Kreuzer et al., 2009). Contributions of each component (air, mantle and crust) in total ^{4}He and ^{3}He budgets are shown in (b) and (c), respectively, based on the mixing relationships shown in (a).

tively, the contributions of each endmember were calculated, and are shown in Fig. 3b and 3c.

It appears that the ^{3}He budget of all groundwater samples is controlled by mantle components admixed with atmospheric ^{3}He, which should be more or less constant (Fig. 3c). The contribution from of crustal ^{3}He is negligible. In contrast, a large part of ^{4}He is derived from crustal components with a limited contribution from mantle derived ^{4}He, up to 6% (Fig. 3b). The largest mantle He contribution is found in the deepest well (700 m) at the eastern edge of the Coastal Plain, either because the sample has received a

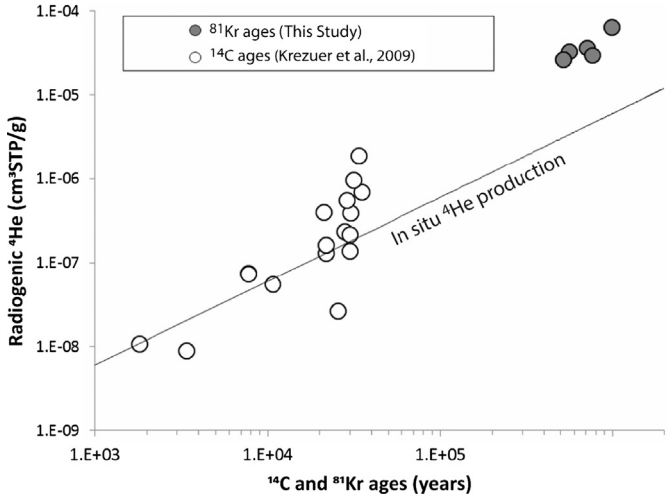

Fig. 4. ^{14}C (Krezuer et al., 2009) and ^{81}Kr ages determined for the NCP groundwater samples plotted against the radiogenic ^{4}He. Radiogenic ^{4}He produced within the aquifer matrix and transferred to groundwater is shown with a reported in situ production rate of 6×10^{-12} cm^3 STP/g/yr (Wei et al., 2015).

larger input of mantle He compared with groundwater from shallower levels, or because it has the longest residence time among the present sample set.

4.3. ^{81}Kr ages

Previous studies on groundwater dating with ^{3}H/^{3}He and ^{14}C methods on the western side of the NCP reveal groundwater ages that are progressively older from the piedmont area of the Taihang Mountains to the east. Kreuzer et al. (2009) also showed ^{4}He concentrations correlated with ^{3}H/^{3}He and ^{14}C ages, suggesting that ^{4}He accumulates with increasing groundwater residence time (Fig. 4). However, it also appears that the correlation becomes uncertain around the 20,000–30,000 yr range due to the detection limit of the ^{14}C method. Thus, ^{14}C is not expected to provide meaningful age information for our samples because they are from sites further east to the Central Plain area. To obtain residence time for much older samples, we collected dissolved gas samples from five separate sites from the Coastal plain area for age determination by ^{81}Kr.

Table 2 shows the results of ^{81}Kr analyses of these samples. ^{81}Kr/Kr ratios in the samples ($= R_{sample}$) range from 5% to 20% of the modern atmospheric ratio ($R_{Air} = (^{81}\mathrm{Kr/Kr})_{Air} = 1.1 \times 10^{-12}$; Du et al., 2003). With the ^{81}Kr decay constant ($\lambda_{\mathrm{Kr}} = 3.03 \times 10^{-6}$ yr^{-1}), the age (t_{Kr}) was calculated using:

$$t_{\mathrm{Kr}} = -\frac{1}{\lambda_{\mathrm{Kr}}} \ln\left(\frac{R_{Sample}}{R_{Air}}\right) \tag{2}$$

The range of ages estimated for these samples was 0.5 to 1.0 Ma and these ^{81}Kr ages correlate with their radiogenic ^{4}He contents (Fig. 4). The oldest among the five samples (NCP-004) is from the easternmost site; the youngest one (NCP-001) is from the westernmost and is 70 km away from the NCP-004 site.

5. Discussion

5.1. Calibration of effective ^{4}He flux using ^{81}Kr ages

We have shown above that there is an increase in ^{4}He concentrations along the flow path (Fig. 2) and that ^{4}He concentrations correlate with ^{81}Kr ages spanning a much older age range than is accessible using the ^{14}C method (Fig. 4). These observations lead to an expectation that ^{4}He concentrations provide a robust age tracer, if the rate at which radiogenic ^{4}He accumulation in the aquifer samples can be constrained.

Radiogenic ^{4}He is produced within aquifers by α-decay of U and Th, and its accumulation rate can be estimated with a knowledge of U and Th elemental contents of aquifer rock matrix, along with the assumption of a complete transfer of radiogenic ^{4}He to groundwater. The simplest approach to estimate groundwater residence times is to assume *in situ* production as the sole source for the observed amount of crustal ^{4}He and to use the production rate as rate constant (e.g., Castro et al., 2000; Kipfer et al., 2002; Wei et al., 2015). However, this often results in overestimation of groundwater ages when compared to residence times determined by other techniques (Aggarwal et al., 2015). In the case of the NCP, the *in situ* production rate of ^{4}He was estimated to be about 6×10^{-12} cm^3 STP/g/yr based on U and Th measurements from sedimentary core samples (Wei et al., 2015). As discussed in Wei et al. (2015), *in situ* ^{4}He can account for observed amounts of radiogenic ^{4}He in samples with ^{14}C ages younger than about (2–3) $\times 10^{4}$ yr (Fig. 4). Geographically, these younger samples are from the Piedmont to the middle of the Central Plain (Longitude $<$ *ca.* 115.5°E). However, for samples with longer residence times, especially those from the Coastal Plain with ^{81}Kr ages of $> 5 \times 10^{5}$ yr, the *in situ* production is insufficient to account for the observed amount of radiogenic ^{4}He (Fig. 4). This discrepancy suggests that the *in situ* component is responsible for only a part of total radiogenic ^{4}He in those samples with relatively larger radiogenic ^{4}He ($>2 \times 10^{-7}$ cm^3 STP/g), and that an external basal ^{4}He flux into the aquifer is required to control the amount of helium in the samples (e.g., Torgersen and Ivey, 1985).

Distribution of radiogenic ^{4}He in an aquifer with two sources (an *in situ* component and an external basal ^{4}He flux) can be modeled as (Torgersen and Ivey, 1985):

$$\left[^{4}\mathrm{He}\right]_{x,z} = \left(\frac{P}{U}\right)x + \left(\frac{F(4\mathrm{He})/\phi}{U}\right)\left[\frac{x}{h} + \left(\frac{hU}{D_{\mathrm{He}}}\right) \times \left\{\frac{3z^2 - h^2}{6h^2} - \frac{2}{\pi^2}\sum_{n=1}^{\infty}\frac{(-1)^n}{n^2}e^{-\frac{D_{\mathrm{He}}n^2\pi^2 x}{h^2 U}}\cos\frac{n\pi z}{h}\right\}\right] \tag{3}$$

where P = production rate of ^{4}He by *in situ* decay, U = horizontal flow velocity, ϕ = porosity of the aquifer, x = distance from the recharge zone, h is thickness of the aquifer, z is a depth of sampling from the aquifer top, and D_{He} is an effective (vertical) helium diffusion coefficient. A basal flux ($F(^{4}\mathrm{He})$) enters the aquifer across its bottom. U denotes a horizontal flow rate of groundwater and is written as x/t with a residence time (t). Some of the parameters, such as an *in situ* ^{4}He production rate (P), can be estimated from U and Th contents of aquifer matrix rock. In the case of the NCP aquifer system, as noted above, previous work reports $P = 6 \times 10^{-12}$ cm^3 STP/g/yr (Wei et al., 2015). Aquifer geometry is also relatively simple for the NCP with its confined layers (layer III–V3) consisting of a thickness of about 950 m and a relatively flat basement at 1050 m b.s.l. Depths of well screens are also known, and porosity is reported to be 0.2 (Zhang et al., 2000). These leaves the effective ^{4}He flux $F(^{4}\mathrm{He})$ and the vertical diffusion coefficient D_{He}, as two variables in the equation (3), that control the model distribution of radiogenic ^{4}He within the NCP aquifer system.

It is also possible to calculate the time for the groundwater at the sampling depth to obtain the observed amount of radiogenic ^{4}He (this required accumulation time will hereafter be called "^{4}He model age"). The ^{4}He model age strongly depends on $F(^{4}\mathrm{He})$ and D_{He}, and differs significantly depending on the depth of samples (namely the z/h ratios). Optimization of $F(^{4}\mathrm{He})$ and D_{He} is possible by minimizing the differences between the ^{4}He model ages

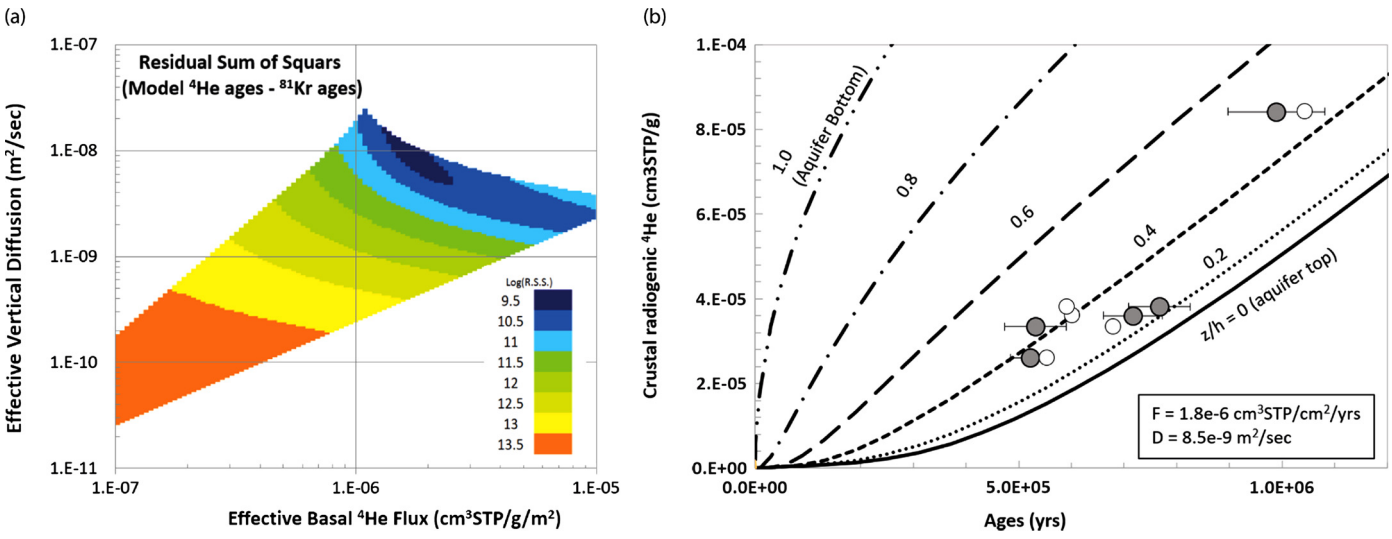

Fig. 5. (a) Residual sum of squares of the model ^{4}He ages and the observed ^{81}Kr ages obtained over ranges of basal effective ^{4}He flux and the effective vertical helium diffusion coefficients. (b) Concentration of crustal radiogenic ^{4}He in the NCP plotted against ^{81}Kr ages (filled circles) and ^{4}He model ages. Curves represent the model concentrations of ^{4}He at given depths and ages in the aquifer (expressed as z/h ratios) determined based on the model of Aggarwal et al. (2015), with the effective ^{4}He flux and diffusion coefficients optimized by using ^{81}Kr ages.

and the observed ^{81}Kr ages (Aggarwal et al., 2015). A set of five ^{4}He model ages (NPC-001 to 005) were calculated for a pair of given $F(^{4}\mathrm{He})$ and D_{He} from $F(^{4}\mathrm{He}) = 10^{-7}$–$10^{-5}$ cm^3 STP/cm^2/yr and $D_{\mathrm{He}} = 10^{-11}$–$10^{-7}$ m^2/s and compared with the ^{81}Kr ages. As shown in Fig. 5a, we find the residual sum of squares between the ^{4}He model ages and the observed ^{81}Kr ages shows a minimum (i.e., best agreement) at $F(^{4}\mathrm{He}) = 1.8 \times 10^{-6}$ cm^3 STP/cm^2/yr and $D_{\mathrm{He}} = 8.5 \times 10^{-9}$ m^2/s. With these fluxes and vertical diffusion, the ^{4}He model ages agree with the observed ^{81}Kr ages within about 30% (Fig. 5b). Fig. 5b displays the degree of concordance between the ^{4}He model ages and ^{81}Kr ages with the optimized values of $F(^{4}\mathrm{He})$ and D_{He}. Considering the large uncertainties in assumed or assigned parameters (e.g., depth of sampling, porosity and aquifer geometry) as well as analytical uncertainty in ^{81}Kr, a robust assessment of the uncertainties in these obtained ^{4}He model ages is not feasible. For now, we assign a 30% error to cover the differences between ages by ^{4}He and ^{81}Kr.

The method described above yields reasonable agreement between ^{81}Kr and ^{4}He chronometers in two separate aquifers – the NCP and Guarani aquifers (Fig. 6), demonstrating that groundwater dating by ^{4}He concentrations can be more quantitative when the model parameters are calibrated by an independent age tracer.

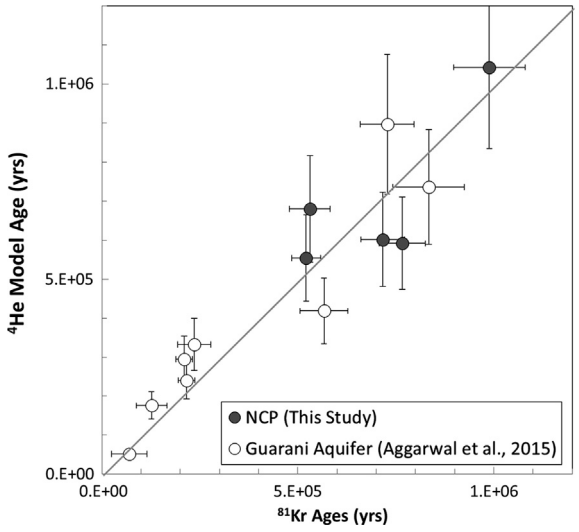

Fig. 6. A comparison between the ^{4}He model ages and the observed ^{81}Kr ages at the optimum effective ^{4}He flux and diffusion coefficient for the NCP samples. For comparison, the ages from the Guarani aquifer (Aggarwal et al., 2015) are also shown. The solid line has a slope of unity and indicates age concordancy.

5.2. Implications for helium fluxes from the mantle and crust

As shown above, calibration of the model parameters with ^{81}Kr reveals an optimum effective ^{4}He flux into the NCP and Guarani aquifers that differs by a factor of 10 (2×10^{-6} cm^3 STP/cm^2/yr for the NCP versus 2×10^{-7} cm^3 STP/cm^2/yr for the Guarani; Aggarwal et al., 2015). Hereafter, we will explore possible mechanisms that could be responsible for the apparent variation in the effective ^{4}He fluxes between the NCP and Guarani aquifers.

A distinct difference between these two sites is the occurrence of mantle-derived helium in the NCP, whereas the Guarani aquifers show no indication of a mantle source. By using the amount of mantle-derived ^{3}He in each sample, and using the same modeling methods (the same set of input parameters as for the case of ^{4}He, but without *in situ* radiogenic ^{3}He production), the effective mantle-^{3}He flux at the base of the NCP aquifer was estimated to be about 10^{-12} cm^3 STP/cm^2/yr ($=8 \times 10^{3}$ atoms/m^2/s). Note that simple diffusion is not likely to deliver ^{3}He from mantle depths to shallow sedimentary strata (Ballentine et al., 2002). The mantle-derived helium component is often found in formations closely associated with specific geological features such as volcanic systems and major faults (e.g., Kennedy et al., 1997), or associated with regions of high heat flow (Matsumoto et al., 2003) and higher extension and shear strain rates (Kennedy and van Soest, 2007). Tectonically, the NCP is known to have undergone several distinct phases of rifting and subsidence during the Mesozoic and Cenozoic eras, and rapid subsidence and widespread calc-alkaline basaltic volcanism, especially during early Tertiary (Ye et al., 1985). The region is also known for highly active intraplate seismicity, with well-developed fault systems (e.g., Guodong, 1987). Moreover, the area with the highest ^{3}He/^{4}He ratios (Longitude of 116° to the east) coincides with one of many small regions with high heat flow anomalies (Hu et al., 2000; Tao and Shen, 2008), scattered widely in the Eastern part of the continent. These geological/tectonic features all support the interpretation that there are pathways in the continental lithosphere beneath the NCP which permit ready access of mantle-derived fluid to the shallower sedimentary basin.

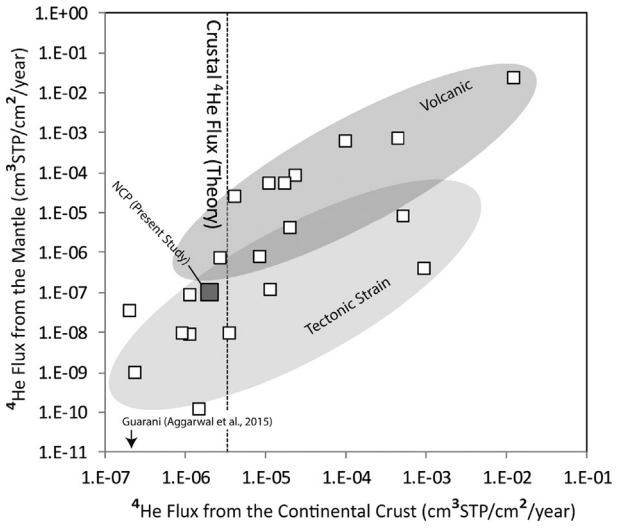

Fig. 7. Fluxes of ^{4}He from the mantle and the continental crust compiled by Torgensen (2010), with the effective crustal and mantle ^{4}He fluxes estimated for the NCP – 2×10^{-6} and 10^{-7} cm^3 STP/cm^2/yr, respectively. The effective crustal ^{4}He flux to the Guarani aquifer (Aggarwal et al., 2015) is also shown by an arrow. (Dark shade: volcanic/magmatic influences. Light shade: area with tectonic strain.)

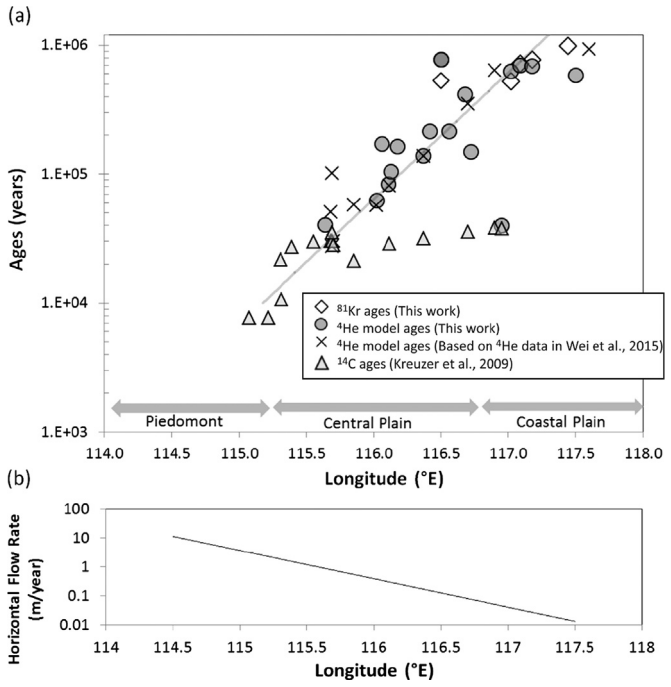

Fig. 8. (a) Isotope ages determined by ^{14}C, ^{81}Kr and ^{4}He in the NCP groundwaters. (b) Horizontal flow rate estimated based on an apparent linear correlation between ages and longitudes in (a).

An important consequence of such a process would be that the upward movement of mantle-derived fluids and/or melts can potentially result in enhanced fluxes of ^{4}He from the continental crust. This is shown in Fig. 7 in which previously reported mantle and crustal He fluxes in areas of tectonic strain and/or magmatic activities are correlated with each other (adopted from Torgensen, 2010), and tend to show that the ^{4}He flux from the crustal source is significantly larger than the theoretical "crustal ^{4}He flux", a diffusion controlled release of radiogenic ^{4}He from continental basement rocks ($=4 \times 10^{-6}$ cm^3 STP/cm^2/yr, based on *in situ* production and steady state release to the atmosphere from the continental crust; e.g., Tolstikhin, 1975; Mamyrin and Tolstikhin, 1984; Torgersen, 1989). The mechanism responsible for coupled and elevated mantle and crustal helium fluxes is uncertain, but we envisage that advective vertical movement of fluids/melts from the mantle effectively scavenges *in situ* radiogenic helium accumulated in the crust through their passage. Consequently, a total ^{4}He flux exiting the continental basement in tectonically active regions, including the NCP, could have been larger than the theoretical "crustal ^{4}He flux.

An additional process that might have limited the effective helium flux at the bottom of the aquifer would be suppression by a non-advective, diffusion/dispersion-controlled transfer of radiogenic ^{4}He through a sedimentary layer between the continental basement rock and the aquifer strata (Aggarwal et al., 2015). In the absence of active and recently active magmatism and/or tectonic activity in the Parana Basin, South America (e.g., Chulick et al., 2013), this diffusion-controlled process appeared to be the primary control on the size of the effective ^{4}He flux entering the Guarani aquifer (Aggarwal et al., 2015). The NCP aquifer overlies a thick sediment layer of ~10 km above the Paleozoic basement (e.g., Yang and Xu, 2004). Thus, the diffusion controlled flux reduction could result in a much smaller effective ^{4}He flux for the NCP. However, in the eastern part of the NCP, the effect of the flux reduction was likely offset by tectonically enhanced ^{4}He exiting from the continental basement, resulting in a larger effective ^{4}He flux than the Guarani aquifer. In contrast, there is no mantle-derived helium observed in groundwater samples from the western part of the NCP (this study, and Wei et al., 2015). Then, the flux reduction through thick sedimentary strata is expected to be a primary process that affects the size of the effective ^{4}He flux in the western part of the NCP. Indeed, as noted earlier, the concentration of ^{4}He in groundwater samples from the western part of the NCP can be accounted for by *in-situ* production within the aquifer, so that the effective ^{4}He flux is negligibly small in the western part (Wei et al., 2015). Hence, there seems to be a divide between the Western and Eastern parts of the NCP in terms of the size of effective helium fluxes into the NCP aquifers. This boundary was clearly delineated by the occurrence of the mantle-derived helium which reflects the tectonic/magmatic conditions within the underlying continental crust.

5.3. Insights from multiple isotopic tracers (^{4}He, ^{14}C and ^{81}Kr)

In order to see the distribution of groundwater ages across the flow path of the NCP, we compiled ages estimated by ^{81}Kr (this study), ^{14}C (Kreuzer et al., 2009) and ^{4}He (^{4}He model ages based on ^{4}He concentrations reported here and in Wei et al., 2015) (Fig. 8a). The model ages were estimated for samples from the eastern part of the NCP, as the application of the ^{4}He flux optimized based on ^{4}He and ^{81}Kr from the eastern part should lead underestimation of ages for samples from the western part of the NCP.

As noted earlier, groundwater residence times are at the ^{14}C detection limit in the middle of the Central Plain, and there is a gap between the ages determined by ^{81}Kr and those reliably dated by ^{14}C (Fig. 4). These ^{4}He model ages cover the gap by extending the trends previously defined by the youngest ages (^{14}C ages with $<10^4$ yr) to the older age range determined by the ^{81}Kr method ($>5 \times 10^5$ yr). This suggests that there is continuity of groundwater flow of the NCP from the recharge zone to the coastal plain area, at least in the deeper confined sections (Section 3 to 5). This finding is in good agreement with a recent conceptual model for the groundwater in the Quaternary and Neogene aquifers in the NCP (Cao et al., 2016).

The apparent correlation of ages and flow distance in the semilogarithmic diagram (Fig. 8a) means that groundwater ages increase exponentially to the east. This further reveals an exponential decrease in the flow rates to the east (Fig. 8b). In an age

range below 10,000 yr in the eastern end of the Piedmont area (Longitude of 115.0 to 115.5°E), ^{14}C ages indicate an eastward component of the flow rate of about 5 m/yr (Kreuzer et al., 2009). In the middle of the Central Plain the flow rate suggested by the ^{4}He model ages is 0.8 to 1 m/yr. Further east in the Coastal Plain, the ^{81}Kr ages define a flow rate of 0.2 m/yr. This dramatic drop in flow rates towards the coastal area should be reflected in a decreased hydraulic gradient and/or continuous drop of permeability, likely reflecting finer deposits in the Neogene aquifers from the central to coastal plains.

6. Conclusion

^{81}Kr age dating carried out on the deep groundwater samples from the Coastal Plain of the North China Plain (NCP) yields ages between 0.5 Ma and 1 Ma. In addition to helium derived from the atmosphere and from the continental crust, groundwater samples from the Central and the Coastal plain areas contain a significant contribution of helium from a mantle reservoir, reflecting the tectonically active nature of the continental crust beneath the NCP. However, because of the significantly larger ^{4}He/^{3}He ratio of the crustal component than the mantle, we can show that >90% of total ^{4}He in the samples is derived from the crust. The crustal component of ^{4}He shows a clear correlation with ^{81}Kr ages, indicating that the radiogenic ^{4}He can be used as an age proxy.

The crustal ^{4}He and ^{81}Kr ages allowed us to estimate the size of the effective ^{4}He flux entering the aquifer as well as the vertical diffusion/dispersion rate of ^{4}He within the aquifer. This allowed us to convert observed ^{4}He concentrations of the radiogenic component in groundwaters from the Central and Coastal plain into residence times (= ^{4}He model ages). The modeling yielded ^{4}He model ages that agree with ^{81}Kr ages, demonstrating the feasibility of our methodology in tectonically active regions, as marked by profound emanation of mantle-derived ^{3}He.

The ^{4}He model groundwater ages from the Central Plain appear to be 5 to 10 times greater than ^{14}C ages, and reveal a clear progression over ~200 km across a flow path from the eastern edge of the Piedmont through the Central Plain to the Coastal plain. This suggests continuity of groundwater flow in the deeper confined sections of the NCP aquifers. Finally, it is becoming clear that the deep groundwater (>300 m) under the central and coastal plains undergoes limited replenishment from flow originating in the piedmont area, and therefore needs to be considered as a non-renewable resource on human timescales.

Acknowledgements

This study was financially supported by the IAEA Coordinated Research Project F33023 (RC No. 20850) and the National Natural Science Foundation of China (No. 41772271 and 21427804). We thank Pradeep Aggarwal who provided insight and expertise that greatly assisted the research. Len Wassenaar is thanked for his comments and efforts to refine English. Yuelong Chen and Zhigang Liang are gratefully acknowledged for providing geological information of the NCP. We thank Derek Vance for the editorial handling of this manuscript as well as three anonymous reviewers for their insightful and thorough reviews.

References

Aeschbach-Hertig, W., 2014. Radiokrypton dating finally takes off. Proc. Natl. Acad. Sci. USA 111 (19), 6856–6857.

Aeschbach-Hertig, W., Stute, M., Clark, J.F., Reuter, R.F., Schlosser, P., 2002. A paleotemperature record derived from dissolved noble gases in groundwater of the Aquia Aquifer (Maryland, USA). Geochim. Cosmochim. Acta 66, 797–817.

Aggarwal, P., Matsumoto, T., Sturchio, N.C., Chang, H.K., Gastmans, D., Araguas-Araguas, L.J., Jiang, W., Lu, Z.T., Mueller, P., Yokochi, R., Purtschert, R., Torgersen, T., 2015. Continental degassing of ^{4}He by surficial discharge of deep groundwater. Nat. Geosci. 8, 35–39.

Andrews, J.N., 1985. The isotopic composition of radiogenic helium and its use to study groundwater movement in confined aquifers. Chem. Geol. 49, 339–351.

Ballentine, C.J., Burgess, R., Marty, B., 2002. Tracing fluid origin, transport and interaction in the crust. In: Porcelli, D., et al. (Eds.), Noble Gases in Geochemistry and Cosmochemistry, vol. 47. Mineralogical Society of America, Washington, pp. 539–614.

Cao, G., Han, D., Currell, M.J., Zheng, C., 2016. Revised conceptualization of the North China Basin groundwater flow system: groundwater age, heat and flow simulations. J. Asian Earth Sci. 127, 119–136.

Castro, M.C., Stute, M., Schlosser, P., 2000. Comparison of ^{4}He ages and ^{14}C ages in simple aquifer systems: implications for groundwater flow and chronologies. Appl. Geochem. 15, 1137e1167.

Chen, Z.Y., Qi, J.X., Xu, J.M., Xu, J.M., Ye, H., Nan, Y.J., 2003. Paleoclimatic interpretation of the past 30 ka from isotopic studies of the deep confined aquifer of the North China plain. Appl. Geochem. 18, 997e1009.

Chulick, G.S., Detweiler, S., Mooney, W.D., 2013. Seismic structure of the crust and uppermost mantle of South America and surrounding oceanic basins. J. South Am. Earth Sci. 42, 260–276.

Dong, Y., He, M., Jiang, S., Wu, S., Jiang, S., 2002. Chloride-36 age study for deep groundwater of Quaternary sediments, Hebei Plain. Earth Sci. 27, 105–109 (in Chinese with English abstract).

Du, X., Purtschert, R., Bailey, K., Lehmann, B.E., Lorenzo, R., Lu, Z.-T., Mueller, P., O'Connor, T.P., Sturchio, N.C., Young, L., 2003. A new method of measuring ^{81}Kr and ^{85}Kr abundances in environmental samples. Geophys. Res. Lett. 30 (20), 2068. https://doi.org/10.1029/2003GL018293.

Graham, D.W., 2002. Noble gas isotope geochemistry of mid-ocean ridge and ocean island basalts; characterization of mantle source reservoirs. In: Porcelli, D., Wieler, R., Ballentine, C. (Eds.), Noble Gases in Geochemistry and Cosmochemistry. Rev. Mineral. Geochem. 47, 247–318. Mineral. Soc. Amer., Washington, D.C.

Guodong, L., 1987. The Cenozoic rift system of the North China Plain and the deep internal process. Tectonophysics 133, 277–285.

Hu, S., He, J., Wang, J., 2000. Heat flow in the continental area of China: a new data set. Earth Planet. Sci. Lett. 179, 407.

Kennedy, B.M., Kharaka, Y.K., Evans, W.C., Ellwood, A., DePaolo, D.J., Thordsen, J., Ambats, G., Mariner, R.H., 1997. Mantle fluids in the San Andreas Fault System, California. Science 278, 1278–1281.

Kennedy, B.M., van Soest, M.C., 2007. Flow of mantle fluids through the ductile lower crust: helium isotope trends. Science 318, 1433–1436.

Kipfer, R., Aeschbach-Hertig, W., Peeters, F., Stute, M., 2002. Noble gases in lakes and ground waters. Rev. Mineral. Geochem. 47, 615–700.

Kreuzer, A.M., von Rohden, C., Friedrich, R., Chen, Z., Shi, J., Hajdas, I., Kipfer, R., Aeschbach-Hertig, W., 2009. A record of temperature and monsoon intensity over the past 40 kyr from groundwater in the North China Plain. Chem. Geol. 259, 168–180.

Kulongoski, J.T., Hilton, D.R., Cresswell, R.G., Hostetler, S., Jacobson, G., 2008. Helium-4 characteristics of groundwaters from Central Australia: comparative chronology with chlorine-36 and carbon-14 dating techniques. J. Hydrol. 348, 176–194.

Lehmann, B.E., Love, A., Purtschert, R., Collon, P., Loosli, H.H., Kutschera, W., Beyerle, U., Aeschbach-Hertig, W., Kipfer, R., Frape, S.K., Herczeg, A., Moran, J., Tolstikhin, I., Gröning, M., 2003. A comparison of groundwater dating with ^{81}Kr, ^{36}Cl and ^{4}He in four wells of the Great Artesian Basin, Australia. Earth Planet. Sci. Lett. 211, 237–250.

Lu, Z.T., Schlosser, P., Smethie, W.M., Sturchio, N.C., Fischer, T.P., Kennedy, B.M., Purtschert, R., Severinghaus, J.P., Solomon, D.K., Tanhua, T., Yokochi, R., 2014. Tracer applications of noble gas radionuclides in the geosciences. Earth-Sci. Rev. 138, 196–214.

Mamyrin, B.A., Tolstikhin, I.N., 1984. Helium Isotopes in Nature. Elsevier, New York. 273 pp.

Matsumoto, T., Kawabata, T., Matsuda, J., Yamamoto, K., Mimura, K., 2003. ^{3}He/^{4}He ratios in well gases in the Kinki district, SW Japan: surface appearance of slab-derived fluids in a non-volcanic area in Kii Peninsula. Earth Planet. Sci. Lett. 216, 221–230.

Matsumoto, T., Solomon, D.K., Araguas-Araguas, L., Aggarwal, P., 2017. The IAEA's coordinated research project on "Estimation of groundwater recharge and discharge by using the tritium, helium-3 dating technique": in lieu of a preface. Geochem. J. 51, 385–390.

Plummer, L.N., Eggleston, J.R., Andreasen, D.C., Raffensperger, J.P., Hunt, A.G., Casile, G.C., 2012. Old groundwater in parts of the upper Patapsco aquifer, Atlantic Coastal Plain Maryland, USA: evidence from radiocarbon, chlorine-36 and helium-4. Hydrogeol. J. 20, 1269–1294.

Purtschert, R., Yokochi, R., Sturchio, N.C., 2013. Krypton-81 dating of old groundwater (Chapter 5). In: Isotope Methods for Dating Old Groundwater, pp. 91–124.

Sturchio, N., Du, X., Purtschert, R., Lehmann, B.E., Sultan, M., Patterson, L.J., Lu, Z., Müller, P., Bigler, T., Bailey, K., O'Connor, T.P., Young, L., Lorenzo, R., Becker, R., El Alfy, Z., El Kaliouby, B., Dawood, Y., Abdallah, A.M.A., 2004. One million year old groundwater in the Sahara revealed by krypton-81 and chlorine-36. Geophys. Res. Lett. 31, L05503.

Suckow, A., Gröning, M., Jaklitsch, M., Han, L-H., Aggarwal, P., 2008. The noble gas facility for isotope hydrology at IAEA, Vienna: goals, technical principles and first results. Geophys. Res. Abstr. 10, EGU2008-A-09357.

Tao, W., Shen, Z., 2008. Heat flow distribution in Chinese continent and its adjacent areas. Prog. Nat. Sci. 18, 843–849.

Tolstikhin, I.N., 1975. Helium isotopes in the Earth's interior and in the atmosphere: a degassing model of the earth. Earth Planet. Sci. Lett. 26, 88–96.

Torgersen, T., 1989. Terrestrial helium degassing fluxes and the atmospheric helium budget: implications with respect to the degassing processes of continental crust. Chem. Geol., Isot. Geosci. Sect. 79, 1–14.

Torgersen, T., 2010. Continental degassing flux of He-4 and its variability. Geochem. Geophys. Geosyst. 11, Q06002.

Torgersen, T., Ivey, G.N., 1985. Helium accumulation in groundwater, II: a model for the accumulation of the crustal ^{4}He degassing flux. Geochim. Cosmochim. Acta 49, 2445–2452.

Tu, L.Y., Yang, G.M., Cheng, C.F., Liu, G.L., Zhang, X.Y., Hu, S., 2014. Analysis of Kr-85 and Kr-81 in a few liters of air. Anal. Chem. 86, 4002–4007.

Wei, W., Aeschbach-Hertig, W., Chen, Z., 2015. Identification of He sources and estimation of He ages in groundwater of the North China Plain. Appl. Geochem. 63, 182–189.

Weiss, R.F., 1968. Piggyback sampler for dissolved gas studies on sealed water samples. Deep-Sea Res. 15, 695–699.

Wen, T., Castro, M.C., Hall, C.M., Pinti, D.L., Lohmann, K.C., 2016. Constraining groundwater flow in the glacial drift and Saginaw aquifers in the Michigan Basin through helium concentrations and isotopic ratios. Geofluids 16, 3–25.

Yang, G.-M., Cheng, C.-F., Jiang, W., Lu, Z.-T., Purtschert, R., Sun, Y.-R., Hu, S.-M., 2013. Analysis of ^{85}Kr: a comparison at the 10–14 level using micro-liter samples. Sci. Rep. 3, 1596. http://doi.org/10.1038/srep01596.

Yang, G.-M., Tu, L.-Y., Cheng, C.-F., Zhang, X.-Y., Hu, S.-M., 2015. Counting radiokrypton atoms with a laser. Chin. J. Chem. Phys. 28, 445–452. http://doi.org/10.1063/1674-0068/28/cjcp1505108.

Yang, Y., Xu, T., 2004. Hydrocarbon habitat of the offshore Bohai Basin, China. Mar. Pet. Geol. 21, 691–708.

Yatsevich, I., Honda, M., 1997. Production of nucleogenic neon in the Earth from natural radioactive decay. J. Geophys. Res. 102 (B5), 10291–10298.

Ye, H., Shedlock, K.M., Hellinger, S.J., Sclater, J.G., 1985. The North China Basin: an example of a Cenozoic rifted intraplate basin. Tectonics 4, 153–169.

Zhang, Z.H., Shen, Z.L., Xue, Y.Q., Ren, F.H., Shi, D.H., Yin, Z.Z., Zhong, Z.S., Sun, X.R., 2000. Evolution of Groundwater and Environment in the North China Plain. Geological Publish House, Beijing, China (in Chinese).